Electrosynthesis of Iminophosphoranes: Accessing P(V) Ligands from P(III) Phosphines

Velabo Mdluli,[1] Dan Lehnherr,[1,*] Yu-hong Lam,[2,*] Mohammad T. Chaudhry,[3] Justin A. Newman,[3] Jimmy O. DaSilva,[3] Erik L. Regalado[3]

[1]Process Research and Development, Merck & Co., Inc., Rahway, New Jersey 07065, United States.
[2]Modeling and Informatics, Merck & Co., Inc., Rahway, New Jersey 07065, United States.
[3]Analytical Research and Development, Merck & Co., Inc., Rahway, New Jersey, 07065, United States.

Keywords: Electrosynthesis, iminophophorane, phosphorus(V), ligands, electrochemistry, catalysis.

ABSTRACT: Iminophosphorane P(V) compounds are accessed via electrochemical oxidation of commercially available P(III) ligands, including mono-, di- and tri-dentate phosphines as well as chiral phosphines. The reaction uses inexpensive bis(trimethylsilyl)carbodiimide as an efficient and safe aminating reagent. DFT calculations, cyclic voltammetry, and NMR spectroscopic studies provide insight into the reaction mechanism. The proposed mechanism based on the data reveals a special case of sequential paired electrolysis, namely a domino electrolysis process in which intermediates generated at the cathode are subsequently oxidized at the anode, followed by an additional convergent paired electrolysis process. DFT calculations of the frontier orbitals of the iminophosphorane are compared to those of the analogous P(III) phosphines and P(V) phosphine oxides. This reveals that *N*-cyano-iminophosphoranes have both a higher HOMO and lower LUMO than their analogous phosphine oxide, rendering them suitable for both σ-donating and π-back-bonding.

Phosphine ligands are ubiquitous in catalysis.[1] Phosphorus(III)-based ligands are synonymous with transition metal catalysis, both in asymmetric hydrogenations and cross coupling chemistries (e.g. C–C, C–N, C–O couplings) using metals like Rh, Ru, Pd to name a few. Phosphines have also been used as organocatalysts, typically for nucleophilic catalysis,[2] while phosphoric acid and related P(V) derivatives are used as organocatalysts for Brønsted acid catalysis or ion-pairing applications.[3] The use of phosphorus(V) ligands is significantly less explored in catalysis.[4] Phosphine mono-oxide ligands have been demonstrated in Pd-couplings (Figure 1A & 1B),[5,6,7,8] as well as asymmetric Cu-catalyzed alkylation of imines and nitroalkenes.[9] P(V) structures have been used directly as the catalyst (i.e. in the absence of a metal). One example is a phosphine oxide catalyzed enantioselective aldol reaction using carboxylic acids and aldehydes shown in Figure 1C.[10] P=S and P=Se based phosphorimides catalysts have been used to mediate per-silylation of 2′-deoxynucleosides to access the corresponding glycal as a result of eliminating the nucleobase (Figure 1D).[11] P(III)/P(V) redox catalysis has been used for amination of boronic acid derivatives from nitroarenes or nitroalkanes, as well as other reactions including the deoxygenative condensation of α-keto esters and carboxylic acids.[12] Examples of incorporating phosphorus in pharmaceutical and agrochemicals, [13] as well as in functional materials are prevalent.[14] For example, phosphine oxides, such as bis{2-[di(phenyl)phosphino]-phenyl}ether oxide (**DPEPO**, Figure 1F), are commonly used as host materials in organic light emitting devices (OLEDs).[15] P(V) functional groups are also featured in pharmaceuticals such as remdesmivir (for the treatment of COVID-19)[16] and risderonate acid (typically used as the sodium salt for the treatment of osteoporosis).[17]

Iminophosphoranes are an underutilized class of P(V) ligands, in which only sparse applications for catalysis have been reported. These include as ligands in cross-coupling reactions (e.g. Sonogashira, Suzuki-Miyaura, and Negishi couplings) and hydrogenations of alkene and ketones,[18] as well as in organocatalysis (Figure 1E),[19] ethylene polymerizations,[20] amongst others.[21] Iminophosphoranes have also been used as organic neutral super-electron donors in organic synthesis.[22] The synthesis of iminophosphoranes typically uses either: (a) a decomposition of an alkyl azide (hazardous) via a Staudinger reaction, or (b) a sequential amination of PCl_5 (the original Kirsanov reaction),[23,24] or (c) a two-step bromination-amination process (the generalized Kirsanov reaction).[25] These methods suffer from hazardous reagents,[26] limited

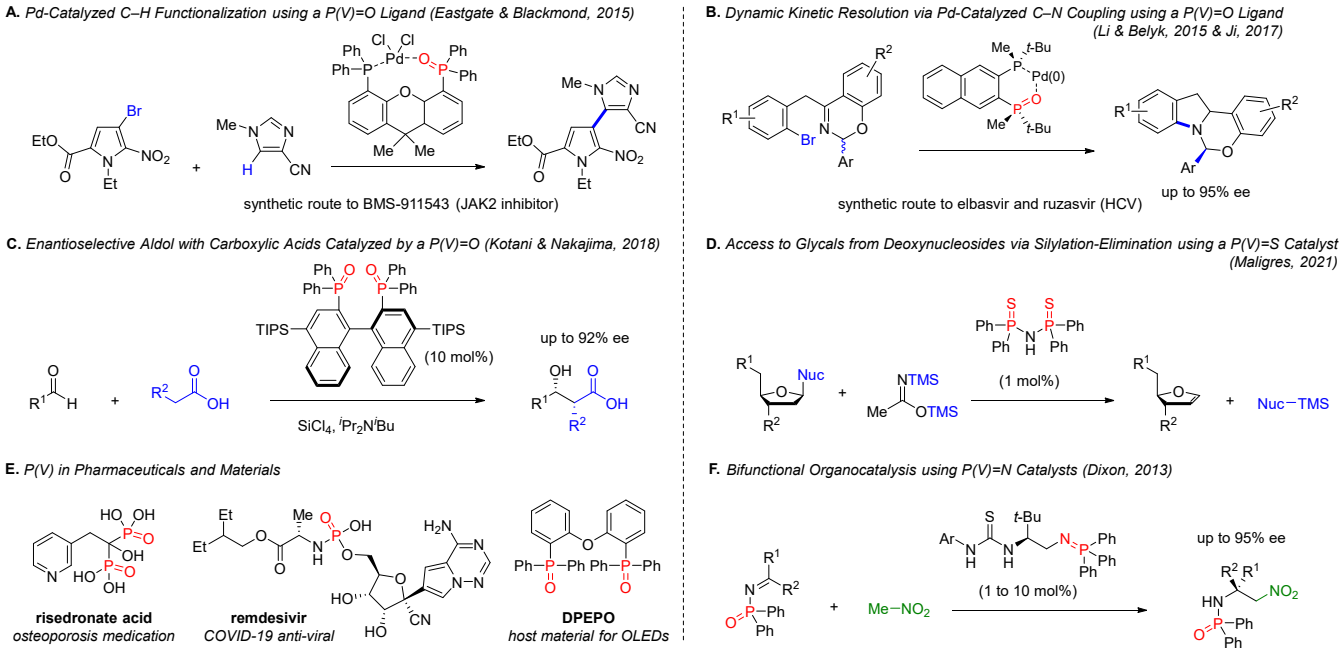

Figure 1. (A–F) Applications of P(V) ligands and catalysts. (F) Structure of P(V) ligands and *N*-cyanoimine derived ligands as inspiration of *N*-cyano iminiophosphoranes. (G) Electrosynthesis of iminophosphoranes from P(III) phosphines (this work).

access to a commercial source of the requisite starting materials, and limitations in their scope. Despite the interesting emerging catalysis based on P(V) ligands and catalysts, access to P(V) structures is still limited, in stark contrast to the hundreds of commercially available P(III) ligands. To address this limitation, we wondered if electrochemistry[27,28] could be used to convert commercially available P(III) ligands to P(V) iminophophorane ligands (Scheme 1A) via an sustainable and safe oxidative process, potentially greatly expanding the chemical space of phosphorus-based ligands available for catalysis.[29] Inspired by the impact of *N*-cyanoimine ligands reported by Weix and Hansen (Scheme 1B),[30] we chose to target *N*-cyano iminophosphoranes (Scheme 1A) for our initial explorations.[31]

More broadly, classic sp²-nitrogen-based ligand scaffolds for base-metal catalysis,[32] like bipyridine (**bipy**), terpyridine (**terpy**), and related structures (see Scheme 1B),[33] were envisioned to be transposed to scaffolds containing iminophosphoranes in which the P=N fragments in structure **IP-1** to **IP-3** serve as an isostere for the C=N fragment of the classic sp²-nitrogen based ligands mentioned above.[34] Herein we report an electrochemical method to access iminophosphoranes and mechanistic studies of this new transformation. This enables single-step access to new ligand chemical space from commercially available phosphines, as well as facile entry into chiral ligands, in contrast to chiral bipyridines, phenanthrolines, and terpyridines.[35]

Scheme 1. (A) Electrosynthesis of Iminophosphoranes from Phosphines (B) Ligand Scaffold Hopping.

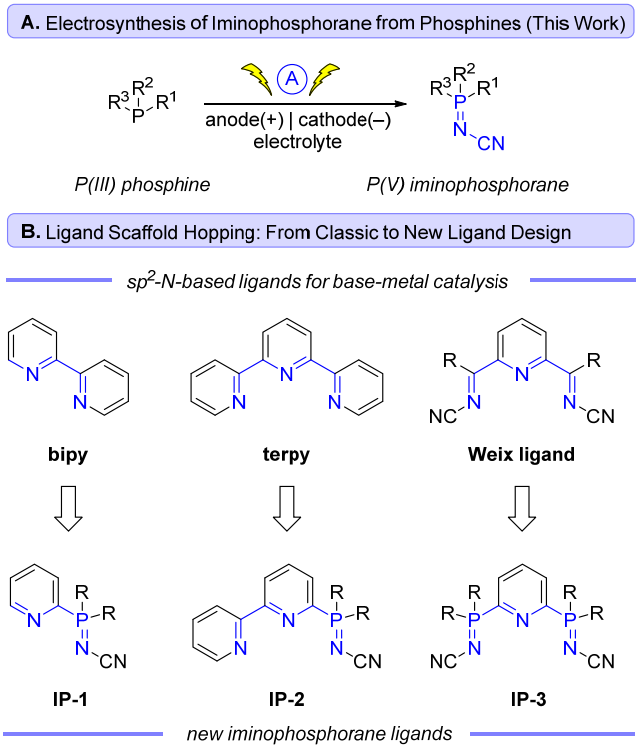

We initially targeted iminophophorane **1** (Figure 2) for the reaction development as it is air stable and has a UV-vis chromophore, thus enabling analysis of reaction mixture

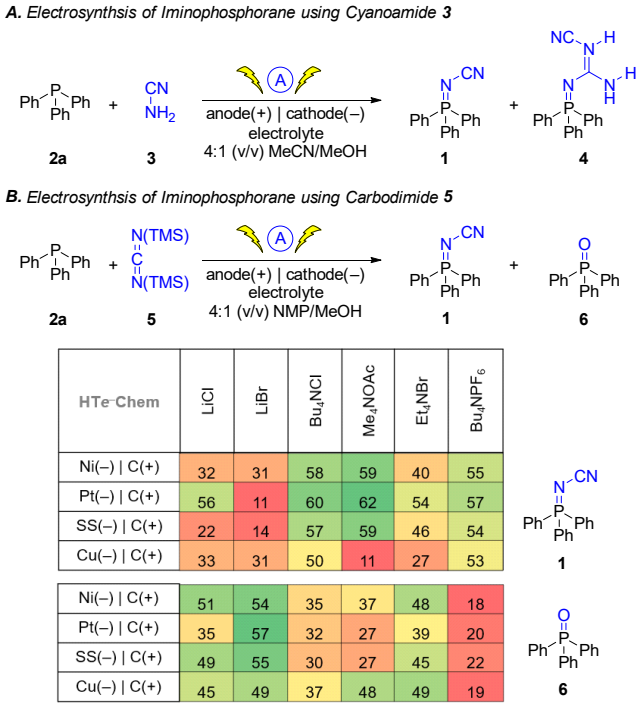

HTe-Chem	LiCl	LiBr	Bu_4NCl	Me_4NOAc	Et_4NBr	Bu_4NPF_6
Ni(–) | C(+)	32	31	58	59	40	55
Pt(–) | C(+)	56	11	60	62	54	57
SS(–) | C(+)	22	14	57	59	46	54
Cu(–) | C(+)	33	31	50	11	27	53

1

Ni(–) | C(+)	51	54	35	37	48	18
Pt(–) | C(+)	35	57	32	27	39	20
SS(–) | C(+)	49	55	30	27	45	22
Cu(–) | C(+)	45	49	37	48	49	19

6

Figure 2. (A) Initial attempts at synthesizing iminophosphorane **1a** using cyanamide. (B) Heat map of assay yields obtained using HT*e*-Chem to screen electrolytes and electrode for the synthesis of iminophosphorane **1a** using bis(trimethylsilyl)carbodiimide). Conditions: 30 μmol scale (0.1 M) using constant current (1 mA) using 2 F/mol charge at room temperature. Note: C = graphite, SS = stainless steel.

via UPLC. Given that the modified Kirsanov reaction uses Br_2 to oxidize PPh_3 to Ph_3PBr_2 followed by amination to access iminophosphoranes, we started off by using bromide containing electrolytes to affect an anodic generation of Br_2 to mediate the oxidation of Ph_3P (**2a**) in the presence of cyanamide (**3**) towards synthesizing iminophosphorane **1** (Figure 2). The use of Et_4NBr as an electrolyte, enabled oxidation of PPh_3 in 4:1 (v/v) MeCN/MeOH provided 15% yield of **1** when using graphite anode and stainless steel cathode and guanidine **4** in 12% yield, which was confirmed by X-ray crystallography (Figure 3). We explored an alternative aminating reagent towards improving the selectivity for iminophosphorane **1** over guanidine **4**. We wondered if a more soluble surrogate for cyanamide, specifically bis(trimethylsilyl)carbodiimide (**5**), would improve the reaction outcome. Indeed, the use of **5** under otherwise identical conditions provided iminophosphorane **1** in 70% yield and no detectable guanidine **4**. We explored these conditions with a handful of other phosphines but soon realized that solubility of the phosphine starting material was poor in a number of examples (e.g. xanthphos). Thus, we replaced MeCN with NMP as a cosolvent to achieve improved solubility, however the yield for **1** dropped to 43%. Given the multi-variable optimization problem, we turned to high throughput experimentation to address this challenge. Using the recently reported[36] and commercialized[37] HT*e*-Chem reactor[38] we explored both electrolyte and electrode variables using 4:1 (v/v) NMP/MeOH as the solvent system. The use of Me_4NOAc as the electrolyte in combination with platinum cathode and graphite anode provided the highest yield of iminophosphorane **1**. The $Ph_3P{=}O$ (**6**) side product is postulated to arise from adventitious water or oxygen in the solvent reacting competitively against the aminating reagent.

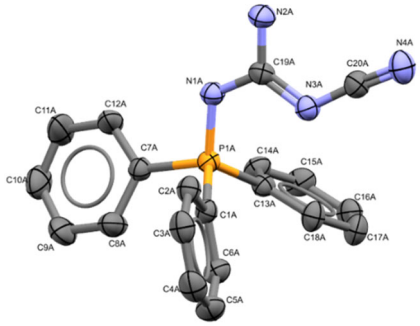

Figure 3. X-ray crystallographic structure of side-product **4** (CCDC 2259467). ORTEP ellipsoid plotted at 50% probability.

Based on reaction optimization using the HT*e*-Chem reactor, the optimal conditions were translated from 30 μmol scale to the Electrasyn 2.0 setup on 2 mmol scale using a current of 10 mA (j = 4.2 cm^2/mA) and a charge of 2.5 F/mol. The choice of NMP and Me_4NOAc also facilitates the reaction workup, as the reaction can be poured into water to precipitate out the desired product in many cases, while leaving the electrolyte in solution. Collection of the crude product via filtration followed by either recrystallization or column chromatography affords the desired products in high purity with a variety of substrates (see Supporting Information for details).

With optimal reaction conditions in hand, we turned our attention to exploring the substrate scope of our electrochemical synthesis of iminophosphoranes (Table 1). We targeted a diverse substrate scope drawing inspiration from phosphine ligands commonly used in cross-coupling reactions, specifically those that are commercially available. Amination of triphenylphosphine on 2 mmol scale provide **1** in 83% yield. Electronically varied triarylphosphines are well tolerated as demonstrated with *para*-substituted analogs of triphenylphosphine: *p*-OMe (**7**) 74% yield, *p*-F (**8**) 92% yield, *p*-Cl (**9**) 73% yield, and *p*-CF_3 (**10**) 83% yield. Styrenyl containing product **11** is obtained in 79% yield, which could have application as a precursor to iminophosphorane-functionalized polystyrene materials (e.g. polystyrene resin-bound ligand/catalyst for heterogenous catalysis).[39] *Ortho*-substitution is well tolerated as demonstrated by being able to access product **12** in 86% yield. Even tertiary amines functionalized phosphine can be carried through the reaction, albeit in diminished yield, as exemplified with an analog of APhos to access **13** in 39% yield.

TABLE 1. Reaction scope for the electrosynthesis of iminiophosphorane.[a]

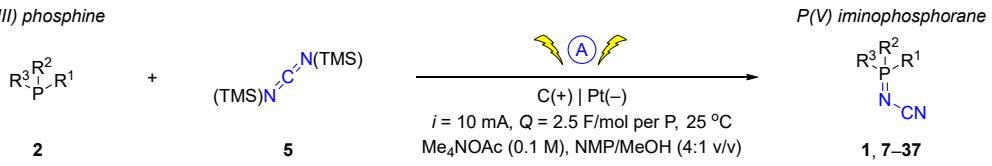

2 **5** **1**, **7**–**37**

monodentate P(V) ligands

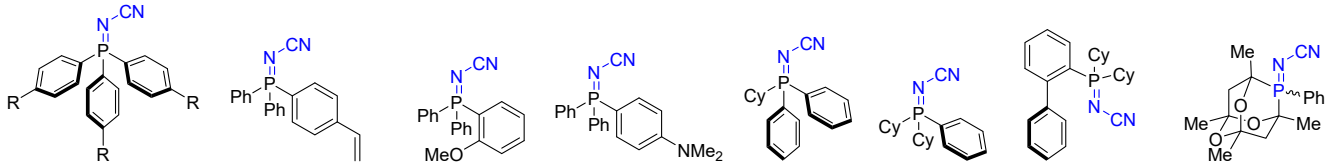

1 R = H 83%
7 R = OMe 74%
8 R = F 92%
9 R = Cl 73%
10 R = CF_3 83%

11 79% *from* 4-(Ph_2P)styrene

12 86% *from* (2-MeO-C_6H_4)PPh_2

13 39% *from* Ph_2-APhos

14 56% *from* $CyPPh_2$

15 82% *from* Cy_2PPh

16 75% *from* CyJohnPhos

17 89% (1:1 dr) *from* ^{me}CgPPh

sp^2-N,P(V) polydentate ligands

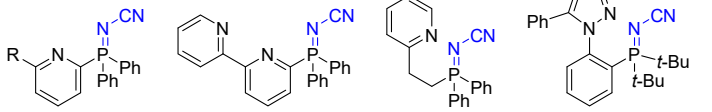

18 R = H, 86%
19 R = Me, 87%

20 83% *from* 2-(Ph_2P)bypy

21 85% *from* DPPPyE

22 81% *from* *t*-Bu-PP-DPPpyrazole

chiral monodentate P(V) ligands

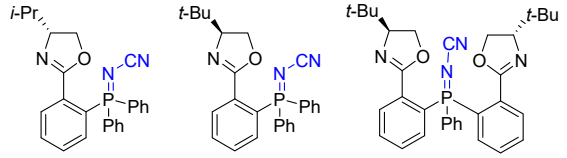

23 70% *from* (*R*)-*i*-Pr-PHOX

24 69% *from* (*S*)-*t*-Bu-PHOX

25 55% *from* (*S*,*S*)-di-*t*-Bu-PHOX

bis-P(V) ligands

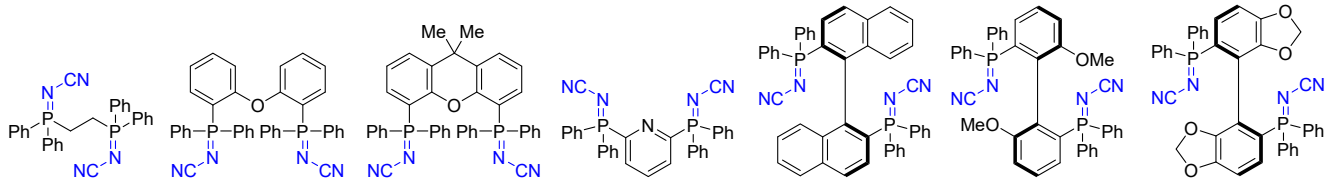

26 87% *from* DPPE

27 63% *from* DPEPhos

28 79% *from* Xantphos

29 68% *from* bis(DPP-Py)

30 62%[b] *from* (*S*)-BINAP

31 68% *from* (*S*)-BIPHEP

32 43% *from* (*R*)-SEGPHOS

tris-P(V) ligands

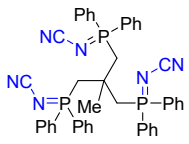

33 44% *from* 1,1,1-Tris(diphenyl phosphinomethyl)ethane

hetero-bis-P(V) & P(III)-P(V) ligands

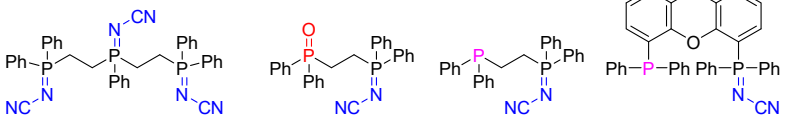

34 74% *from* Bis(2-diphenylphosphinoethyl) phenylphosphine

35 76% *from* DPPE-monooxide

36 32%[c] *from* DPPE

37 34%[c] *from* Xantphos

guanidine derivative

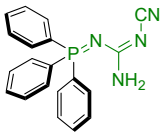

4 49%[d] *from* PPh_3 *using cyanoguanidine instead of* **5**

[a]Standard condition: 2.0 mmol of phosphine (0.13 M) in 4:1 v/v NMP/MeOH containing 6.0 mmol of **5** per phosphorus, and 1.5 mmol of Me_4NOAc; constant current electrolysis (10 mA, j = 4.2 mA/cm^2) and a charge of 2.5 F/mol per phosphorus using a graphite anode and a platinum foil cathode. [b]1 mmol scale (0.07 M in phosphine using 14:1 v/v NMP/MeOH containing 1.5 mmol of Me_4NOAc. [c]Same as standard conditions, except 6.0 mmol of **5** was used and the charge was 2.5 F/mol. [d]Same as standard conditions, except 6.0 mmol of *N*-cyanoguanidine was used instead of **5**.

Diarylmonoalkylphosphines are also suitable substrates, as iminophosphorane **14** is accessed in 56% yield from diphenylcyclohexylphosphine. Conversion of dicyclohexylphenylphosphine to **15** is achieved in high yield (82%). The conversion of CyJohnPhos to **16** in 75% yield demonstrates that *ortho*-arylation on phenyl ring is tolerated with

these dialkylmonoarylphoshine substrates. Even acetals can be carried through this transformation as showcased with the functionalization of the ^{me}CgPPh ligand to product **17** in 89% yield (1:1 d.r.).

The incorporation of heterocycles into the iminophosphorane product can be achieved as well as demonstrated with products (**18–22**). The incorporation of pyridyl fragments is demonstrated with both triaryl and diarylposphines with products **18** (86% yield), **19** (87% yield), **20** (83% yield), and **21** (85% yield). Product **22** is obtained in 81% yield, highlighting how a pyrazole can also be brought through this transformation, potentially providing bidentate functionality. Chiral phosphine ligands, such as those based on phosphinooxazolines (PHOX) substructures, can be transformed to their corresponding iminophosphoranes. This was exemplified with products **23–25** that were obtained in yields ranging from 55**–**70%, without evidence of ee erosion.

Bidendate phosphines such as DPPE, DPEPhos, and Xantphos provide **26**–**28** in 87%, 63%, and 79% yield, respectively. 2,6-Bis(diphenylphosphino)pyridine is used to make **29** in 68% yield, providing a tridentate ligand based on three sp^2-nitrogens. Privileged chiral ligand[40] BINAP is converted to its iminophosphorane analog **30** in 62%. Similarly, popular BIPHEP and SEGPHOS ligand scaffolds are used to access **31** and **32** in 68% and 43% yields, respectively.

Tripodal ligands are useful in coordination chemistry and catalysis as the ligand can occupy one face of an octahedral geometry, providing a fixed facial (*fac*) geometry with the opposite face available for catalysis. Thus, we explored the use of commercially available tridentate "triphos"[41] ligands which enabled access to tris(iminophosphorane) ligand **33** and **34** in 44% yield and 74% yield, respectively. These ligands are envisioned to be useful for tripodal complex formation, a strategy that is often used with first-row transition metals.[42]

Access to hetero-bis-phosphine derivatives was explored as illustrated with products **35**–**37**. Two strategies were utilized depending on the target: (1) starting from bis-phosphine mono-oxides, or (2) passing slightly more charge (i.e. 2.5 F/mol) than the theoretical minimum charge of 2 F/mol to oxidize one of the two phosphines. Mixed PO/PN bis-P(V) ligand **35** was accessed starting from the commercially available DPPE-mono-oxide (i.e. P(III)-P(V) monoxide). In contrast, mixed P(III)-P(V) DPPE ligands **36** and **37** were obtained by passing only 2.5 F/mol of charge under otherwise identical conditions to those employed in Table 1.

Finally, returning to the side-product **4** that was obtained during the reaction optimization work, we wondered if inexpensive *N*-cyanoguanidine, commonly used as a fertilizer on large scale,[43] could be utilized in our reaction as the aminating reagent. Gratifyingly, the formation of iminophosphorane **4** containing cyanoguanidine was achieved in 49% yield.

To give the reader a flavor of the kinetic stability of the iminophosophoranes in Table 1, these were typically isolated via either precipitation from the crude reaction mixture using water or subjected to an aqueous workup, in either case typically followed by silica gel column chromatography all in the presence of air. This highlights both their air stability and their resistance towards hydrolysis.

In order to gain mechanistic insight into the reaction, we conducted DFT calculations and followed up with a series of experiments based on NMR spectroscopy (^{1}H, ^{13}C, ^{31}P) and cyclic voltammetry. Five potential mechanisms were initially considered (Scheme 2). In mechanism 1 (Scheme 2A), a pre-equilibrium chemical step precedes the initial oxidation. Specifically, nucleophilic attack of carbodiimide **5** by phosphine **2a** would lead to zwitterionic intermediate **38a** followed by an oxidation to afford distonic radical cation[44] **39a**, which upon fragmentation affords *N*-centered radical **40** (stepwise formal 1,2-shift of the phosphine). Radical **40** could react with phosphine **2a–b** to generate **41a** followed by oxidation to get to **42a**. Alternatively, radical **39** could directly generate **42a** via coupling with the radical cation of the phosphine (**43a**) generated via anodic oxidation from the corresponding phosphine (radical-radical reactions are statistically less likely, especially when neither is a persistent radical). Finally, loss of the silyl group from **42a** would then afford iminophosphorane product **44a**.

In mechanism 2 (Scheme 2B), oxidation of the phosphine (**2a** → **43a**) followed by attack of the carbodiimide **5**, would afford intermediate **39a**, with subsequent steps being identical to mechanism 1.

In mechanism 3 (Scheme 2C), oxidation of bis(trimethylsilyl)carbodiimide **5** would afford distonic radical cation **45**/**45'**, which upon loss of TMS–OMe would afford **40**, thereby once again ultimately leading to product via the identical final steps of mechanism 1.

In mechanism 4 (Scheme 2D), hydrogen evolution at the cathode via reduction of protons from methanol would generate methoxide that could attack a silicon in bis(trimethylsilyl)carbodiimide **5** to generate pentacoordinate silicate anion **46** followed by loss of TMS–OMe to afford anion **47**. Oxidation of anion **47** would generate the key *N*-centered radical **40**, en route to product **44a–b** via the identical final pathway as shown in mechanism 1.

In mechanism 5 (Scheme 2E), methoxylation of bis(trimethylsilyl)carbodiimide at the carbon of the diimide results in either intermediate **48** or **49**, depending on whether MeOH or methoxide is the nucleophile. These two pathways can converge at intermediate **49** which could subsequently generate key anion **47** via loss of TMS–OMe which intercepts mechanism 4 to ultimately lead to the iminophosphorane product **44a**–**b** via radical **40**. Alternatively, oxidation of **49** to **50** and subsequent loss of TMS–OMe leads to radical **40**. Finally, intermediate **48** can also lead to key intermediate **40** via trimethysilylcyanamide **51**. Ultimately, more than one pathway may exist but all of them funnel through intermediate **40** en route to iminophosphorane product **44a**–**b**.

To summarize, the key question related to identifying the operating mechanism is focused on what is the initial step: an oxidation (e.g. oxidation of carbodiimide **5**) or a chemical step (e.g. pre-equilibrium formation of **38**).

Scheme 2. Various reaction mechanisms initially considered (data supports mechanisms D & E).

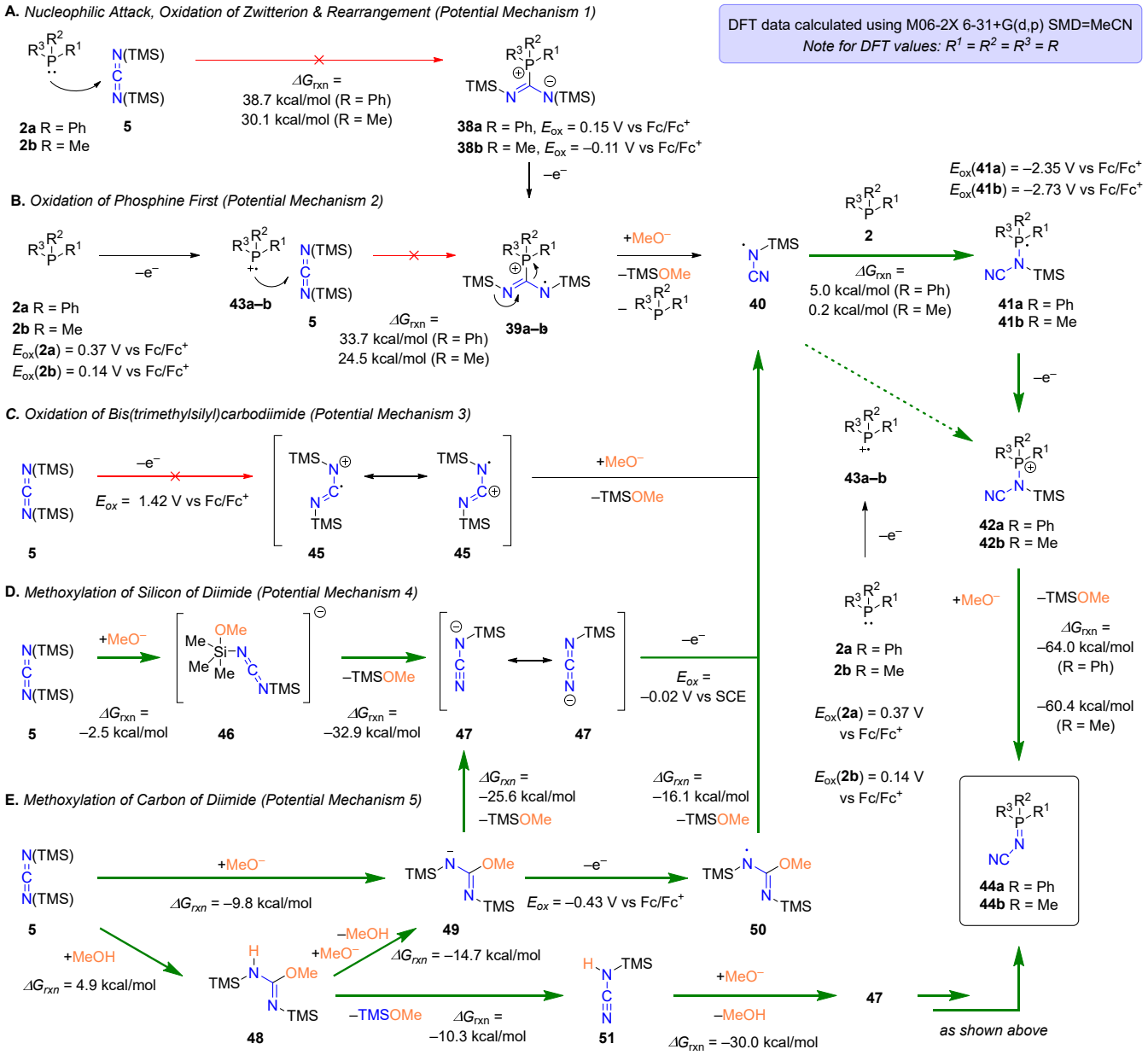

To probe mechanism 1, specifically the feasibility of a pre-equilibrium step to form zwitterion **38** via nucleophilic attack of the carbodiimide **5** by the phosphine, we conducted DFT calculations using M06-2X/6-31+G(d,p) SMD=MeCN.[45] DFT results suggest that phosphine addition to carbodiimide **5** is endothermic and energetically inaccessible at room temperature: 38.7 kcal/mol for PPh_3, 30.1 kcal/mol for PMe_3 (a more electron rich & more nucleophilic trialkylphosphine compared to PPh_3). Experimentally, ^{31}P NMR spectroscopic experiments are consistent with the lack of forming zwitterion **38** (or any new species containing phosphorus). Specifically, no new ^{31}P signals were observed when comparing the ^{31}P NMR spectra for the following three mixtures (all in 4:1 (v/v) NMP/CD_3OH with $(PhO)_3PO$ internal standard): (mixture 1) triphenylphosphine; (mixture 2) triphenylphosphine and 0.1 M Me_4NOAc electrolyte; and (mixture 3) a 3:1 molar ratio of bis(trimethylsilyl)carbodiimide **5** and triphenylphosphine in 0.1 M Me_4NOAc 4:1 (v/v) NMP/CD_3OD.

Finally, cyclic voltammetry (CV) experiments (*vide infra*) of these mixtures of triphenylphosphine and bis(trimethylsilyl)carbodiimide **5** did not reveal the emergence of a redox event at a lower potential than that for PPh_3 (Figure 5). Based on the data from DFT, NMR spectroscopy, and CV experiments we ruled out mechanism 1 formation of zwitterion **38** prior to electrolysis. However, a new oxidation wave was observed around 0.17 V vs Fc/Fc^+ when KOEt was added to solutions of the carbodiimide **5**, which is not present in the cyclic voltammogram of either of the individual components. The alkoxide was added as a

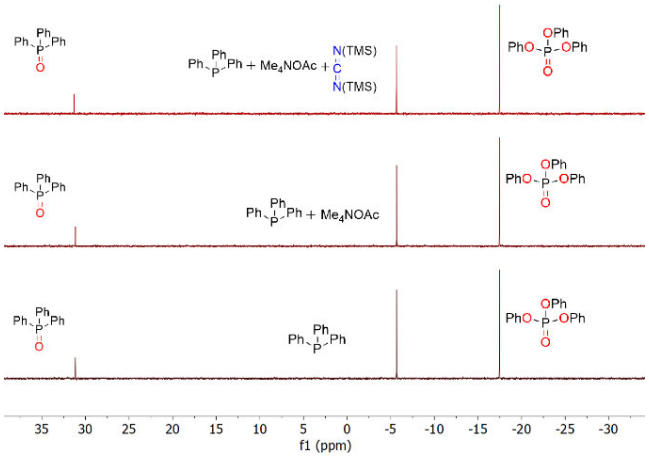

Figure 4. ^{31}P NMR spectra of (top) mixture of triphenylphosphine and bis(trimethylsilyl)carbodiimide (1:3 molar ratio) in 0.1 M Me_4NOAc electrolyte, (middle) triphenylphosphine and 0.1 M Me_4NOAc electrolyte (bottom) triphenylphosphine. All samples are in 4:1 (v/v) NMP/CD_3OD containing $(PhO)_3P=O$ internal standard. Note: samples were prepared in air and contain triphenylphosphine oxide.

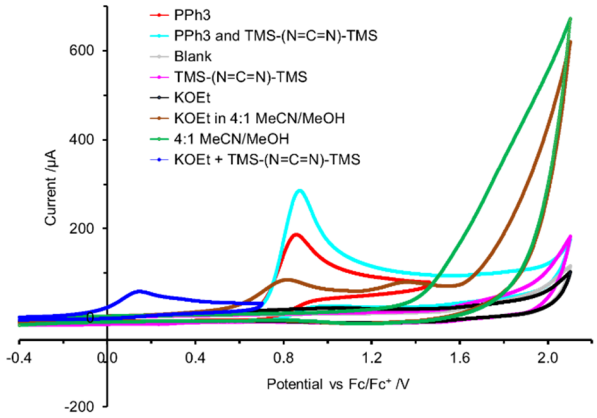

Figure 5. Overlayed cyclic voltammograms of various components containing 0.1 M Bu_4NPF_6 in MeCN measured vs Fc/Fc^+ (ν = 500 mV/s, glassy carbon working electrode, Pt wire counter electrode). See Supporting Information for details.

surrogate for the electrogenerated base at the cathode upon reducing H^+ (from MeOH) to hydrogen. The above CV data supports the alkoxide mediated formation of anion **47** which can be oxidized to the *N*-centered radical **40** (DFT predicted oxidation at –0.02 V vs Fc/Fc^+, vide infra).

DFT calculations can predict oxidation potential as to which compound is easier to oxidize. Calculations[46,47] using M06-2X/6-31+G(d,p) SMD=MeCN predict the following oxidation potentials (all vs Fc/Fc^+): 0.37 V for Ph_3P, 1.42 V for bis(trimethylsilyl)carbodiimide **5**, 1.24 V for Ph_3P=N-CN (**1**) ,and 1.74 for Ph_3P=O (**6**). Cyclic voltammetry[48] provides experimental insight into which compound is easier to oxidize: the phosphine, the bis(trimethylsilyl)carbodiimide (**5**), or the mixture of the above two reagents (which would be consistent with oxidation of zwitterion **38**). Cyclic voltammetry reveals that the oxidation of PPh_3 occurs at 0.76 V vs Fc/Fc^+, >1.5 V vs Fc/Fc^+ for bis(trimethylsilyl)carbodiimide **5**, and 0.79 V vs Fc/Fc^+ for the 1:1 mixture of PPh_3 and **5** (essentially within experimental error of that observed for PPh_3 alone). These data suggest that mechanisms 2, 4 or 5 could be operational (Schemes 2B & 2D), as these do not involve direct oxidation of bis(trimethylsilyl)carbodiimide **5**, unlike mechanism 3 (Scheme 2C).

DFT calculations of the ΔG_{rxn} for 1st step of mechanism 1 or the 2nd step of mechanism 2 have large endothermic values and thus are prohibitive for a room temperature reaction. This suggests that neither of these mechanisms are operational, leaving only mechanism 4 and 5 as feasible mechanisms.

In support of mechanisms 4 and 5 (Scheme 2D & 2E), the omission of methanol results in significantly decreased reaction performance (12% of product **1a**). On the other hand, the identity of the alcohol is less critical other aliphatic alcohols provide iminophosphorane **1a**: EtOH (87%), *t*-amyl alcohol (82%) all give comparable yield to using MeOH (83%) when used in 4:1 v/v MeCN/ROH ratios under conditions otherwise identical to the optimal conditions. Even the use of electron-deficient alcohols (weakly nucleophilic alkoxides) such as trifluoroethanol (TFE) and hexafluoropropanol (HFIP) result in comparable product yields of **1** (91% and 82% respectively). We note that adventitious water may be reduced at the cathode to generate hydroxide which could play a role similar to the alkoxides generated from the alcohols above and may be associated with the 12% yield of **1** when an alcohol is omitted.

While both the DFT and experimental (CV, NMR spectroscopy, and control electrosynthetic experiments) are consistent with mechanisms 4 and 5, there could be two potential pathways from key intermediate **40** to the iminophosphorane product **44**. Either the *N*-centered radical **40** adds to the neutral phosphine **2a** or to the singly oxidized phosphine (i.e. radical cation **43a**). Addition of **40** to neutral phosphines is thermally accessible (ΔG_{rxn} = 5.0 kcal/mol for triphenylphosphine and ΔG_{rxn} = 0.2 kcal/mol for trimethylphosphine), while oxidation of PPh_3 (**2a**) is more challenging (0.37 V Fc/Fc^+) than oxidation of **47** (–0.11 V vs Fc/Fc^+), suggesting that addition of **40** occurs to the neutral phosphine. Subsequent oxidation of the resulting radial intermediate **41a** is facile (–2.35 V vs Fc/Fc^+) thus access to **42a** is facile. Finally, loss of TMS from **43a** provides desired product **44a** with an associated ΔG_{rxn} = –64.0 kcal/mol when R = Ph.

Scheme 3 illustrates the overall electrolysis process based on the proposed mechanism. Reduction of methanol at the cathode generates hydrogen with methoxide as a byproduct which attacks diimide **5**, which upon loss of TMS–OMe generates anion **47**. Oxidization of **47** leads to *N*-centered radical **40**. Subsequent attack of phosphine (2) generates **41** which is immediately oxidized to **42**. Generation of a 2nd equivalent of methoxide, analogous to above, enables breakdown of **42** to generate the desired iminophosphorane product **44** and a 2nd equivalent of TMS–OMe. To the best of our knowledge this represents a rare example of a domino electrolysis reaction,[49,50] which could be categorized as a sequential paired electrolysis followed by a convergent paired electrolysis.[27a,51]

Scheme 3. Proposed mechanism of domino-electrolysis.

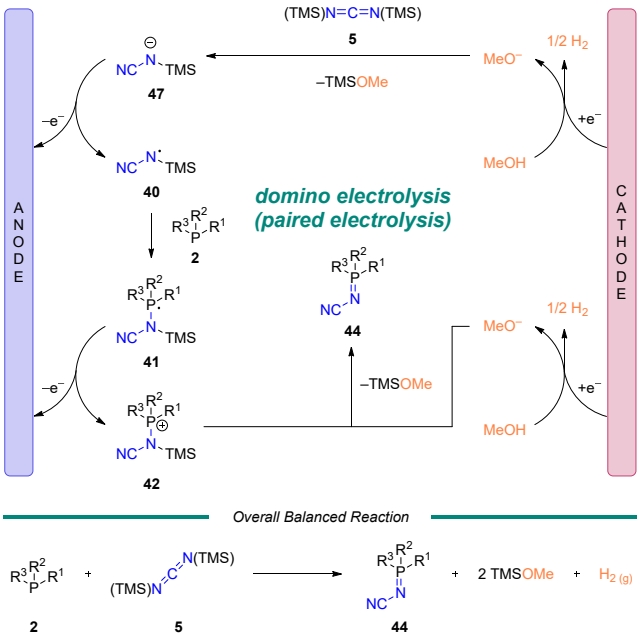

To gain insight into electronic effects of modifying P(III) ligands into their analogous P(V) structures (*N*-cyanoiminophosphorane and phosphine oxide), we computed their frontier molecular orbitals and oxidation potentials using M06-2X/6-31+G(d) SMD=MeCN. Figure 6A illustrates the HOMO and LUMO orbitals for Ph_3P, Ph_3P=N–CN, and Ph_3P=O. The HOMO energy decreases monotonically from –7.31 eV (Ph_3P) to –7.55 eV (Ph_3P=N–CN) to –8.48 eV (Ph_3P=O); all values are versus vacuum. Interestingly, the distribution of the HOMO changes upon these structural variations. Specifically, HOMO is localized on the phosphorus (lone pair) in Ph_3P, but for Ph_3P=O it is delocalized on two of its phenyl rings. Conversely, the HOMO is localized on the N–CN fragment for Ph_3P=N–CN. The DFT predicted oxidation potential (E_{ox}) follows this same trend as the HOMO energies, specifically, E_{ox} = 0.37 V for Ph_3P, 1.24 V for Ph_3P=N–CN, and 1.74 V for Ph_3P=O, all versus Fc/Fc^+). The distribution of the LUMO also vary across these three ligands (thus potentially impacting how back-bonding from a transition-metal to these ligands may occur if they are ligated to a metal). Noteworthy, the LUMO energies do not decrease monotonically when considering the ligands in the same order as above, specifically the LUMO energy varies from –0.01 eV (Ph_3P) to –0.58 eV (Ph_3P=N–CN) to –0.15 eV (Ph_3P=O); all values are versus vacuum. The HOMO-LUMO gap for these three ligands varies from 7.31 eV for Ph_3P to 8.33 eV for Ph_3P=N–CN and 8.32 eV for Ph_3P=O. The reduced HOMO-LUMO gap for Ph_3P=N–CN is mostly due to a more significant lowering of the LUMO in comparison with other structure in that series. Overall, these changes highlight that formal oxidation of the P(III) ligands to P(V) results not only in significant electronic changes, but also that these changes may be different depending on the which group is attached to the P(V) center (O for a phosphine oxide or N–CN for an *N*-cyanoiminiophosphorane).

The classic method of characterizing electronic properties of phosphine ligands is to report the Tolman electronic parameter (TEP).[52] The TEP is the IR frequency associated with the A_1 stretch of the CO for a $Ni(CO)_3L$ complex. The TEP correlates with the electron donating ability of a ligand. DFT calculations provide a quick way of rank ordering a series of ligands and benchmarking studies have validated this approach.[53] Based on these precedents, we computed the TEP for Ph_3P, Ph_3P=O, and Ph_3P=N–CN and obtained 2067.4 cm^{-1}, 2070.1 cm^{-1}, and 2071.6 cm^{-1}, respectively (Figure 6B). The three data point all have similar TEP values, yet may suggest that the iminophosphorane is slightly more electron deficient than the analogous P(III) phosphine.[54] While the DFT calculations show the HOMO is destabilized in the iminophosphoranes compared to the analogous P(III) ligands, suggesting weaker σ-donor ability, the lowering of the LUMO in the iminophosphoranes has the added benefit of being able to participate in improved π-back-bonding (Figure 6).[55] This may have important implications towards stabilizing low-oxidation state transition-metal complexes (e.g. those in a d^{10} configuration) for new or improved catalysis (e.g. Ni-catalyzed cross-coupling reactions).

To probe structural aspects of these new iminophosphoranes, a number of ligands (**13**, **22**, (*R*)-**23**, **26**, **27**, (*S*)-**31**, **35**, and **36**) were crystallized and characterized by X-ray crystallography (Figure 7). Key structural parameters are summarized in the Supporting Information (see Table S10). The bent nature of the "P=N–CN" fragment was indeed confirmed with a typical bond angle associated with the P=N–C fragment being ca. 124°. The average P=N bond length for these eight X-ray crystallographic structures was 1.60 Å, noticeably longer than a P=O bond (1.46 Å) found in triphenylphosphine oxide.[56] The P–C bond length of these iminophosphorane is also influenced compared to that found in triphenylphosphine oxide (1.76 Å).[56] Finally, the stereochemistry of chiral iminophosphorane (*R*)-**23** and (*S*)-**31** are consistent with overall retention based on the starting material used in their electrochemical synthesis.

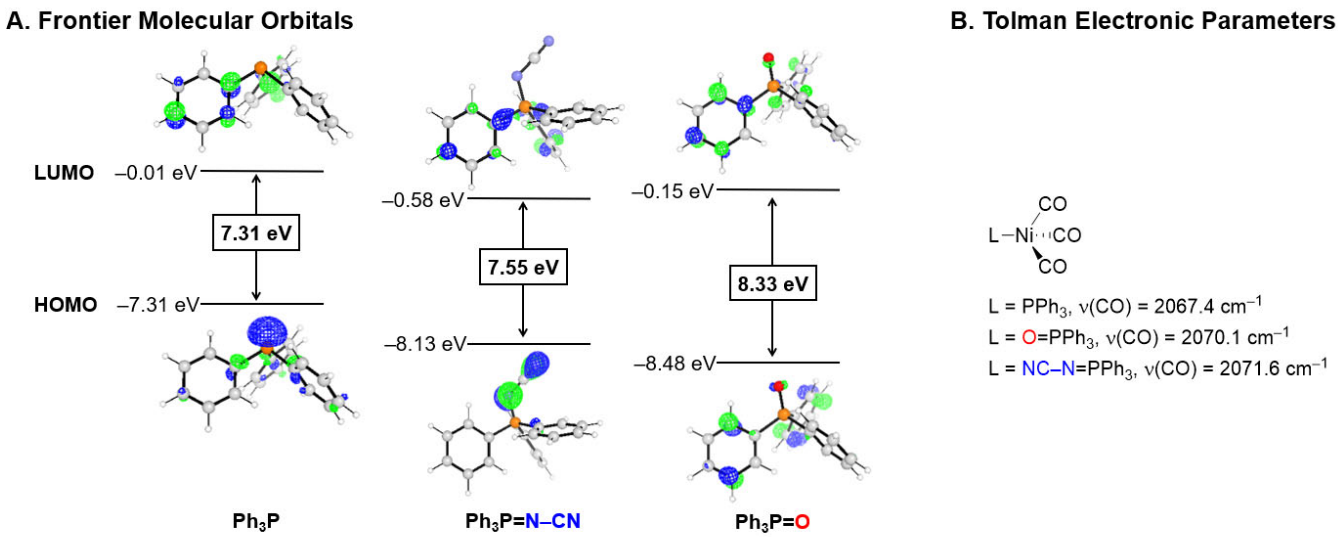

Figure 6. (A) DFT computed lowest unoccupied molecular orbital (LUMO, (top) and highest occupied molecular orbital (HOMO) (bottom) for: (left) PPh_3, (left) $Ph_3P{=}O$, (left) $Ph_3P{=}N{-}CN$, using M06-2X/6-31+G(d) SMD=MeCN. (Note: orbitals are plotted using isolvalue = 0.075 a.u.) (B). Tolman electronic parameters obtained from DFT calculations using MPW1PW91 functional and the following basis sets: 6-311+G(2d) for Ni and 6-311+G(d,p) for all other atoms.

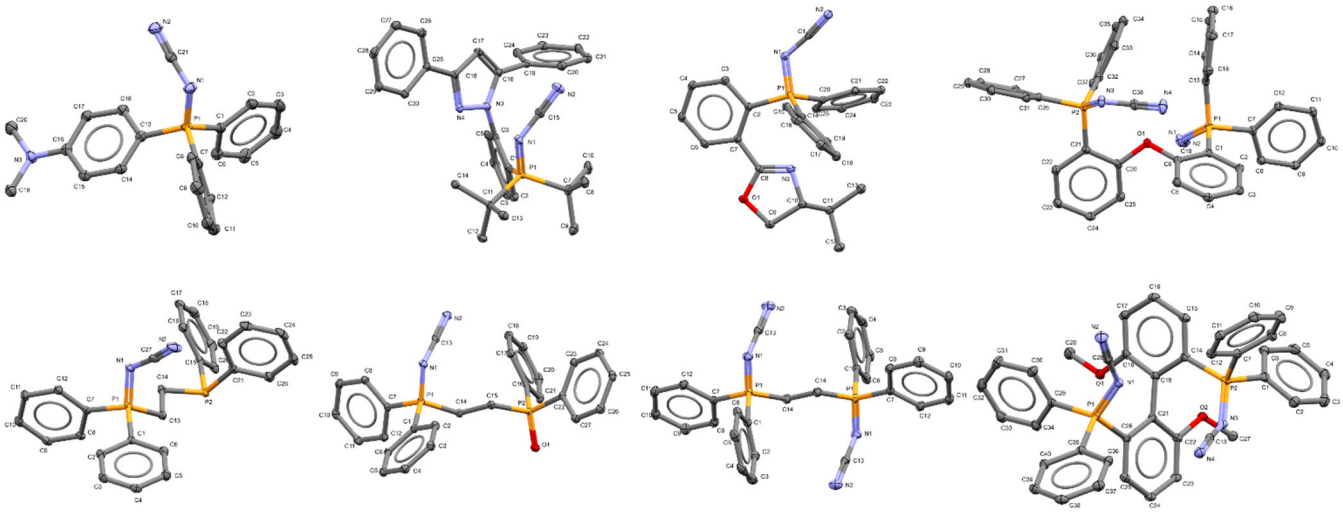

Figure 7. X-ray crystallographic structure of iminophosphorane, (top row, left to right): **13** (CCDC 2258974), **22** (CCDC 2258975), (*R*)-**23** (CCDC 2259466), **27** (CCDC 2258980); (bottom row, left to right)**: 36** (CCDC 2258979), **35** (one of two inequivalent geometries, CCDC 2258978), **26** (CCDC 2258976), and (*S*)-**31** (CCDC 2258977). Note: ORTEP ellipsoid plotted at 50% probability.

To demonstrate both the scalability of the electrochemical synthesis of iminophosphoranes and the accessibility to ligand **26**, we translated our batch electrosynthetic conditions to flow conditions (Scheme 5). Utilizing a parallel plate reactor equipped with carbon felt on graphite as the anode and a Pt cathode, we operated this flow electrolysis reactor in recirculating mode. By switching the electrolyte from Me_4NOAc to the more soluble Bu_4NOAc, and using carbon felt on graphite as the anode instead of graphite (increasing the surface area), we were able to increase the current density from 4.2 to 8.0 mA/cm^2, and ultimately increase productivity. The use of 5.20 F/mol of charge provided complete consumption of both the starting material (**DPPE**) and the P(III)-P(V)-intermediate **36**. The crude reaction mixture was simply diluted with water to induce a direct crystallization from the reaction mixture to isolate **26** (81% isolated yield, corrected for purity).

Scheme 5. Multi-Gram-Scale Flow-Electrosynthesis of Ligand 25.

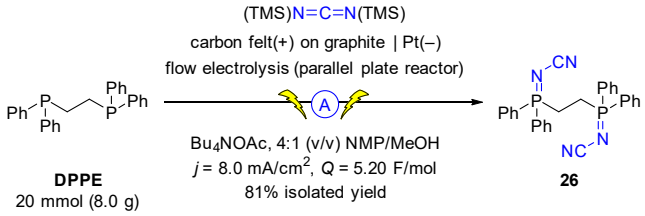

In conclusion, we have developed an operationally simple and safe electrochemical synthesis of new iminophos-

phorane ligands form commercially available phosphine. The mechanistic study reveals a paired-electrolysis mechanism is operational where an electrogenerated base[57] triggers the formation of a key intermediate to enable a rare example of domino electrolysis. This synthetic method provide a safer alternative to conventional Staudinger chemistry (herein we would have required the use of cyanogen-azide, NC–N_3, which is extremely hazardous due to its energetic nature, in fact it is a primary explosive).[58] We are currently evaluating these ligands for transition-metal catalysis and anticipate broad applicability where sp^2-nitrogen based ligands have traditionally been used (e.g. C–N, C–O, C–C). Applications of this electrosynthetic method to synthesize organocatalysts for anion-binding is also envisioned.[19] Impact beyond catalysis with these iminophosphoranes, such as in host materials for OLEDs as replacement for phosphine oxides[59] (e.g. DPEPO), is also envisioned given their promising photostability.

AUTHOR INFORMATION

Corresponding Author

* yu-hong.lam@merck.com
* dan.lehnherr@merck.com

ACKNOWLEDGMENT

V.M. and M.T.C. acknowledge support from the Postdoctoral Fellowship program at Merck & Co., Inc., Rahway, NJ, USA. We thank François Lévesque, Charles Yeung, and Eric Phillips (all at Merck & Co., Inc., Rahway, NJ, USA) for insightful discussions and feedback.

ABBREVIATIONS

bipy, 2,2′-bipyridine; C, graphite; COD, cyclooctadiene; CV, cyclic voltammetry; DFT, density functional theory; dtbbpy, 4,4′-di-*tert*-butyl-2,2′-dipyridyl ; DQ, duroquinone; Fc, ferrocene; Fc^+, ferrocerium; JAK2, Janus kinase 2; HCV, hepatitis C virus; HFIP, hexafluoroisopropanol; HOMO, highest occupied molecular orbital; LUMO, lowest unoccupied molecular orbital; NMP, *N*-methylpyrrolidine; PHOX, phosphinooxazolines; SCE, standard calomel electrode; SS, stainless steel; TBADT, tetrakis(tetrabutylammonium)decatungstate; TEP, terpy, 2,2';6',2"-terpyridine; Tolman electronic parameter; TFE, trifluoroethanol, TMS, trimethylsilyl; ttbtpy, 4″-tri-*tert*-butyl-2,2′:6′,2″-terpyridine.

REFERENCES

[1] (a) Clevenger, A. L.; Stolley, R. M.; Aderibigbe, J.; Louie, J. Trends in the Usage of Bidentate Phosphines as Ligands in Nickel Catalysis. *Chem. Rev.* **2020**, *120*, 6124–6196. (b) Smith, M. B. Phosphorus Ligands. Reference Module in Chemistry, Molecular Sciences and Chemical Engineering. 2013. DOI: 10.1016/B978-0-12-409547-2.01037-4. (c) E. I. Musina, A. S. Balueva and A. A. Karasik, Tertiary Phosphines: Preparation, in *Organophosphorus Chemistry* 2022, *51*, 1–61. DOI: 10.1039/9781839166198-00001.

[2] Hongchao Guo, H.; Fan, Y. C.; Sun, Z.; Wu, Y.; Kwon, O. Phosphine Organocatalysis. *Chem. Rev.* **2018**, *118*, 10049–10293.

[3] Parmar, D., Raja, S., Rueping, M. Complete Field Guide to Asymmetric BINOL-Phosphate Derived Brønsted Acid and Metal Catalysis: History and Classification by Mode of Activation; Brønsted Acidity, Hydrogen Bonding, Ion Pairing, and Metal Phosphates. *Chem. Rev.* **2014**, *114*, 9047–9153.

[4] Yamagiwa, N.; Tian, J.; Matsunaga, S.; Shibasaki, M. Catalytic Asymmetric Cyano-Ethoxycarbonylation Reaction of Aldehydes using a YLi_3Tris(binaphthoxide) (YLB) Complex: Mechanism and Roles of Achiral Additives. *J. Am. Chem. Soc.* **2005**, *127*, 3413–3422.

[5] Ji, Y.; Li, H.; Hyde, A. M.; Chen, Q.; Belyk, K. M.; Lexa, K. W.; Yin, J.; Sherer, E. C.; Williamson, R. T.; Brunskill, A. Ren, S.; Campeau, L.C.; Davies, I. W.; Ruck, R. T. A rational pre-catalyst design for bis-phosphine mono-oxide palladium catalyzed reactions. *Chem. Sci.* **2017**, *8*, 2841–2851.

[6] (a) Ji, Y.; Plata, E. P.; Regens, C. S.; Hay, M.; Schmidt, M.; Razler, T.; Qiu, Y.; Geng, P.; Hsiao, Y.; Rosner, T.; Eastgate, M. D.; Blackmond, D. G. Mono-Oxidation of Bidentate Bisphosphines in Catalyst Activation: Kinetic and Mechanistic Studies of a Pd/Xantphos-Catalyzed C–H Functionalization. *J. Am. Chem. Soc.* **2015**, *137*, 13272–13281. (b) Fox, R. J.; Cuniere, N. L.; Bakrania, L.; Wei, C.; Strotman, N. A.; Hay, M.; Fanfair, D.; Regens, C.; Beutner, G. L.; Lawler, M.; Lobben, P.; Soumeillant, M. C.; Cohen, B.; Zhu, K.; Skliar, D.; Rosner, T.; Markwalter, C. E.; Hsiao, Y.; Tran, K.; Eastgage, M. D. C–H Arylation in the Formation of a Complex Pyrrolopyridine, the Commercial Synthesis of the Potent JAK2 Inhibitor, BMS-911543. *J. Org. Chem.* **2019**, *84*, 4661–4669.

[7] Murray, J. I.; Zhang, L.; Simon, A.; Elipe, M. V. S.; Wei, C. S.; Caille, S.; Parsons, A. T. Kinetic and Mechanistic Investigations to Enable a Key Suzuki Coupling for Sotorasib Manufacture—What a Difference a Base Makes. *Org. Process Res. Dev.* **2023**, *27*, 198–205.

[8] (a) Denmark, S. E.; Smith, R. C.; Tymonko, S.A. Phosphine Oxides as Stabilizing Ligands for the Palladium-Catalyzed Cross-Coupling of Potassium Aryldimethylsilanolates. *Tetrahedron* **2007**, *63*, 5730–5738. (b) King, A. K.; Brar, A. A tertiary phosphine oxide ligand-based recyclable system for the Suzuki-Miyaura and Negishi reactions: Evidence for pseudo-homogeneous catalysis. *Catal. Sci. Technol.* **2023**, *13*, 301–304.

[9] Côté, A. (*R,R*)-Me-DuPHOS Monoxide. *e-EROS Encycl. Reagents Org. Synth.* **2010**, DOI: 10.1002/047084289X.rn01242

[10] Kotani, S.; Yoshiwara, K.; Ogasawara, M.; Sugiura, M.; Nakajima, M. Catalytic Enantioselective Aldol Reactions of Unprotected Carboxylic Acids under Phosphine Oxide Catalysis. *Angew. Chem. Int. Ed.* **2018**, *26*, 15877–15881.

[11] Organocatalytic Conversion of Nucleosides to Furanoid Glycals. Mao, E.; Chung, C. K.; Ji, Y.; Lam, Y-h.; Maligres, P. E. *J. Org. Chem.* **2021**, *86*, 7529–7536.

[12] (a) Hong, S. Y;. Radosevich, A. T. Chemoselective Primary Amination of Aryl Boronic Acids by P^{III}/P^{V}=O-Catalysis: Synthetic Capture of the Transient Nef Intermediate HNO. *J. Am. Chem. Soc.* **2022**, *144*, 8902–8907. (b) Li, G.; Kanda, Y.;

Hong, S. Y.; Radosevich, A. T. Enabling Reductive C–N Cross-Coupling of Nitroalkanes and Boronic Acids by Steric Design of $P^{(III)}/P^{(V)}$=O Catalysts. *J. Am. Chem. Soc.* **2022**, *144*, 8242–8248. (c) Lipshultz, J. M.; Radosevich, A. T. Uniting Amide Synthesis and Activation by P^{III}/P^{V}-Catalyzed Serial Condensation: Three-Component Assembly of 2-Amidopyridines. *J. Am. Chem. Soc.* **2021**, *143*, 14487–14494. (d) Li, G.; Miller, S. P.; Radosevich, A. T. P^{III}/P^{V}=O-Catalyzed Intermolecular N–N Bond Formation: Cross-Selective Reductive Coupling of Nitroarenes and Anilines. *J. Am. Chem. Soc.* **2021**, *143*, 14464–14469. (e) $P^{(III)}/P^{(V)}$-Catalyzed Methylamination of Arylboronic Acids and Esters: Reductive C−N Coupling with Nitromethane as a Methylamine Surrogate. Gen Li, Ziyang Qin, and Alexander T. Radosevich, A. T. *J. Am. Chem. Soc.* **2020**, *142*, 16205–16210. (f) Lim, S.; Radosevich. Round-Trip Oxidative Addition, Ligand Metathesis, and Reductive Elimination in a P^{III}/P^{V} Synthetic Cycle. *J. Am. Chem. Soc.* **2020**, *142*, 16188–16193. (g) Li, G.; Nykaza, T. V.; Cooper, J. C.; Ramirez, A.; Luzung, M. R.; Radosevich, A. T. An Improved P^{III}/P^{V}=O-Catalyzed Reductive C–N Coupling of Nitroaromatics and Boronic Acids by Mechanistic Differentiation of Rate- and Product-Determining Steps. *J. Am. Chem. Soc.* **2020**, *142*, 6786–6799. (h) Nykaza, T. V.; Li, G.; Yang, J.; Luzung, M. R.; Radosevich, A. T. P^{III}/P^{V}=O-Catalyzed Cascade Synthesis of N-Functionalized Azaheterocycles. *Angew. Chem. Int. Ed.* **2020**, *59*, 4505–4510.

[13] (a) Yu, H.; Yang, H.; Shi, E.; Tang, W. Development and Clinical Application of Phosphorus-Containing Drugs. *Med. Drug Discovery* **2020**, 100063. (b) Rodriguez, J. B.; Gallo-Rodriguez, C. The Role of the Phosphorus Atom in Drug Design. *ChemMedChem* **2019**, *14*, 190–216. (c) DiRocco, D. A.; Ji, Y.; Sherer, E. C.; Klapars, A.; Reibarkh, M.; Dropinski, J.; Mathew, R.; Maligres, P.; Hyde, A. M.; Limanto, J.; Brunskill, A.; Ruck, R. T. Campeau, L.-C.; Davies, I. W. A multifunctional catalyst that stereoselectively assembles prodrugs. *Science* **2017**, *6336*, 426–430.

[14] Ung, S. P.-M.; Li, C.-J. From rocks to bioactive compounds: a journey through the global P(V) organophosphorus industry and its sustainability. *RSC. Sustain.* **2023**, *1*, 11–37.

[15] (a) Miao, Y.; Yin, M. Recent progress on organic light-emitting diodes with phosphorescent ultrathin (<1nm) light-emitting layers. *iScience* **2022**, *25*, 103804. (b) Han, C.; Zhao, Y.; Xu, H.; Chen, J.; Deng, Z.; Ma, M.; Li, Q.; Yan, P. A Simple Phosphine–Oxide Host with a Multi-insulating Structure: High Triplet Energy Level for Efficient Blue Electrophosphorescence. *Chem Eur. J.* **2011**, *17*, 5800–5803. (c) Zhang, Q.; Komino, T.; Huang, S.; Matsunami, S.; Goushi, K. Triplet Exciton Confinement in Green Organic Light-Emitting Diodes Containing Luminescent Charge-Transfer Cu(I) Complexes. *Adv. Funct. Mater.* **2012**, *22*, 2327–2336.

[16] Stevens,A. C.; Brak, K.; Bremner, W.; Brown, A. M.; Chtchemelinine, A.; Heumann, L.; Kerschen, J. A.; Subotkowski, W.; Vieira, T.; Wolfe, L. C.; Xu, B.; Yu, C.-Y. Development of a Scalable Lanthanide Halide/Quaternary Ammonium Salt System for the Nucleophilic Addition of Grignard Reagents to Carbonyl Groups and Application to the Synthesis of a Remdesivir Intermediate. *Org. Process Res. Dev.* **2022**, *26*, 754–763.

[17] Crandall, C. Risedronate: A Clinical Review. *Arch Intern Med.* **2001**, *161*, 353–360.

[18] García-Álvarez, J.; García-Garrido, S. E.; Cadierno, V. Iminophosphorane–phosphines: Versatile ligands for homogeneous catalysis. *J. Organomet. Chem.* **2014**, *751*, 792–808

[19] (a) Bifunctional Iminophosphorane Organocatalysts for Enantioselective Synthesis: Application to the Ketimine Nitro-Mannich Reaction Núñez, M. G.; Farley, A. J. M.; Dixon, D. J. *J. Am. Chem. Soc.* **2013**, *135*, 16348−16351. (b) Formica, M.; Rozsar, D.; Su, G.; Farley, A. J. M.; Dixon, D. J. Bifunctional Iminophosphorane Superbase Catalysis: Applications in Organic Synthesis. *Acc. Chem. Res.* **2020**, *53*, 2235–2247. (c) Gao, X.; Han, J.; Wang, L. Design of Highly Stable Iminophosphoranes as Recyclable Organocatalysts: Application to Asymmetric Chlorinations of Oxindoles. *Org. Lett.* **2015**, *17*, 4596−4599. (d) Richard, N. A.; Charlton, G. D.; Dyker, C. A. Enhancing catalytic activity of pyridines via *para*-iminophosphorano substituents. *Org. Biomol. Chem.* **2021**, *19*, 9167–9171. (e) Formica, M.; Rogova, T.; Shi, H.; Sahara, N.; Ferko, B.; Farley, A. J. M.; Christensen, K. E.; Duarte, F.; Yamazaki, K. Catalytic enantioselective nucleophilic desymmetrization of phosphonate esters. *Nat. Chem.* **2023**, DOI: 10.1038/s41557-023-01165-6.

[20] Bézier, D.; Daugulis, O.; Brookhart, M. Polymerization of Ethylene Catalyzed by Phosphine-Iminophosphorane Palladium Complexes. *Organometallics* **2017**, *36*, 2947–2951.

[21] García-Garrido, S. E.; Soto, A. P.; García-Álvarez, J. Chapter Three - Iminophosphoranes (R_3P=NR′): From terminal to multidentate ligands in organometallic chemistry. *Adv. Organomet. Chem.* **2022**, *77*, 105–168.

[22] Hanson, S. S.;Doni, E.; Traboulsee, K. T.; Coulthard, G.; Murphy, J. A.; Dyker, A. Pushing the Limits of Neutral Organic Electron Donors: A Tetra(iminophosphorano)-Substituted Bispyridinylidene. *Angew. Chem. Int. Ed.* **2015**, *54*, 11236–11239.

[23] I. N. Zhmurova and A. V. Kirsanov, *J. Gen. Chem. (USSR) (Engl. Transl.)* **1960**, *30*, 3018.

[24] A. W. Johnson. *Ylides and Imines of Phosphorus.* J. Wiley & Sons, New York, 1993.

[25] Chapter 6: Iminophosphoranes and their Applications. In *Organophosphorus Reagents: A Practical Approach in Chemistry (The Practical Approach in Chemistry Series), 1st Edition*, (Murphy, P. J., Ed.); 2004, Oxford University Press.

[26] For example, the ligands reported herein would have required the use of cyanogen azide ($NC–N_3$) which is highly explosive, typically only handled in dilute solutions (which have short half-lives) rendering the use of this azide both impractical and highly hazardous.

[27] (a) Tay, N. E. S.; Lehnherr, D.; Rovis, T. Photons or Electrons? A Critical Comparison of Electrochemistry and Photoredox Catalysis for Organic Synthesis. *Chem. Rev.* **2022**, *122*, 2487–2649. (b) Yan, M.; Kawamata, Y.; Baran, P. S. *Chem. Rev.* **2017**, *117*, 13230–13319. (c) Wiebe, A.; Gieshoff, T.; Mohle, S.; Rodrigo, E.; Zirbes, M.; Waldvogel, S. R. Electrifying Organic Synthesis. *Angew. Chem. Int. Ed.* **2018**, *57*, 5594–5619. (d) Cohen, B.; Lehnherr, D.; Sezen-Edmonds, M.;

Forstater, J. H.; O'Fredrick, M.; Deng, L.; Ferretti, A. C. Harper, K.; Diwan, M. *Chem. Eng. Res. Des.* **2023**, *192*, 622–637.

[28] Klein, M.; Waldvogel, S. R. Anodic Dehydrogenative Cyanamidation of Thioethers: Simple and Sustainable Syanthesis of *N*-Cyanosulfilimines. *Angew. Chem. Int. Ed.* **2021**, *60*, 23197–23201.

[29] Gensch, T.; dos Passos Gomes, G.; Friederich, P.; Peters, E.; Gaudin, T.; Pollice, R.; Jorner, R.; Nigam, A.; Lindner-D'Addario, M.; Sigman, M. S.; Aspuru-Guzik, A. A Comprehensive Discovery Platform for Organophosphorus Ligands for Catalysis. *J. Am. Chem. Soc.* **2022**, *144*, 1205–1217.

[30] (a) Coupling of Challenging Heteroaryl Halides with Alkyl Halides via Nickel-Catalyzed Cross-Electrophile Coupling. *J. Org. Chem.* **2017**, *82*, 7085–7092. (b) Kim, S.; Goldfogel, M. J.; Gilbert, M. M.; Weix, D. J. Nickel-Catalyzed Cross-Electrophile Coupling of Aryl Chlorides with Primary Alkyl Chlorides. *J. Am. Chem. Soc.* **2020**, *142*, 9902–9907.

[31] For an example of nickel-catalyzed C-C couplings using iminophosphorane ligands, see: Cheisson, T.; Cao, T.-P.-A.; Le Goff, X. F.; Auffrant, A. Nickel Complexes Featuring Iminophosphorane−Phenoxide Ligands for Catalytic Ethylene Dimerization. *Organometallics* **2014**, *33*, 6193–6399.

[32] (a) Buono, F.; Nguyen, T.; Qu, B.; Wu, H.; Haddad, N. Recent Advances in Nonprecious Metal Catalysis. *Org. Process Res. Dev.* **2021**, *25*, 1471–1495. (b) Haibach, M. C.; Shekhar, S.; Ahmed, T. S.; Ickes, A. R. Recent Advances in Nonprecious Metal Catalysis. *Org. Process Res. Dev.* **2023**, *27*, 423–447. (c) Singer, R. A.; Monfette, S.; Bernhardson, D.; Tcyrulnikov, S.; Hubbell, A. K.; Hansen, E. C. Recent Advances in Nonprecious Metal Catalysis. *Org. Process Res. Dev.* **2022**, *26*, 3204–3215. (d) Chirik, P. J.; Engle, K. M.; Simmons, E. M.; Wisnieski, S. R. Collaboration as a Key to Advance Capabilities for Earth-Abundant Metal Catalysis. *Org. Process Res. Dev.* **2023**, DOI: 10.1021/acs.oprd.3c00025. (e) Yang, Q.; Zhao, Y.; Ma, D. Cu-Mediated Ullmann-Type Cross-Coupling and Industrial Applications in Route Design, Process Development, and Scale-up of Pharmaceutical and Agrochemical Processes. *Org. Process Res. Dev.* **2022**, *26*, 1690–1750.

[33] (a) Fache, F.; Shultz, E.; Tommasino, M. L.; Lemaire, M. Nitrogen-Containing Ligands for Asymmetric Homogeneous and Heterogeneous Catalysis. *Chem. Rev.* **2000**, *100*, 2159–2232. (b) Bipyridine: The Most Widely Used Ligand. A Review of Molecules Comprising at Least Two 2,2'-Bipyridine Units. Kaes, C.; Katz, A.; Hosseini, M. W. *Chem. Rev.* **2000**, *100*, 3553–3590. (c) Panicker, R. R.; Remarkably flexible 2,2′:6′,2″-terpyridines and their group 8–10 transition metal complexes – Chemistry and applications. *Coord. Chem. Rev.* **2022**, *459*, 214426. (d) Constable, E. C.; Housecroft, C. E. The Early Years of 2,2′-Bipyridine—A Ligand in Its Own Lifetime. *Molecules* **2019**, *24*, 3951.

[34] For selected examples of other new ligand designs, see: Na, H.; Mirica, L. M. Deciphering the mechanism of the Ni-photocatalyzed C–O cross-coupling reaction using a tridentate pyridinophane ligand. *Nat. Commun.* **2022**, *13*, 1313.

[35] (a) Chelucci, G.; Thummel, R. P. Chiral 2,2'-Bipyridines, 1,10-Phenanthrolines, and 2,2':6',2''-Terpyridines: Syntheses and Applications in Asymmetric Homogeneous Catalysis. *Chem. Rev.* **2002**, *102*, 3129–3170. (b) Bolm, C.; Ewald, M.; Felder, M.; Schlingloff, G. Enantioselective Synthesis of Optically Active Pyridine Derivatives and C2-Symmetric 2,2′-Bipyridines. *Chem. Ber.* **1992**, *125*, 1169–1190.

[36] Rein, J.; Annand, J. R.; Wismer, M. K.; Fu, J.; Siu, J. C.; Klapars, A.; Strotman, N. A.; Kalyani, D.; Lehnherr, D.; Lin, S. Unlocking the Potential of High-Throughput Experimentation for Electrochemistry with a Standardized Microscale Reactor. *ACS Cent. Sci.* **2021**, *7*, 1347–1355.

[37] "HT*e*⁻Chem Electrochemistry", Analytical Sales and Services, Inc. https://www.analytical-sales.com/product-category/photoredox-parallel-synthesis/hte-chem-electrochemistry/ (Accessed April 15, 2023).

[38] Rein, J.; Lin, S.; Kalyani, D.; Lehnherr, D. High-Throughput Experimentation for Electrochemistry. *In The Power of High-Throughput Experimentation*; Leitch, D. C., Jouffroy, M., Emmert, M.; Eds; ACS Symposium Series, Vol. 1419; American Chemical Society, **2023**; pp 167–187. DOI: 10.1021/bk-2022-1419.ch010.

[39] (a) Cozzi, F. Immobilization of Organic Catalysts: When, Why, and How. *Adv. Synth. Catal.* **2006**, *348*, 1367–1390. (b) Itsuno, S.; Haraguchi, N. Chpater 2: Catalysts Immobilized onto Polymers. In *Catalyst Immobilization: Methods and Applications*, Benaglia, M.; Puglis, A., Eds.; Wiley, **2019**. DOI: 10.1002/9783527817290.ch2.

[40] (a) *Privileged Chiral Ligands and Catalysts*; Zhou, Q.-L.; Ed.; Wiley, **2011**. DOI: 10.1002/9783527635207. (b) Yoon, T. P.; Jacobsen E. N. Privileged Chiral Catalysts. *Science* **2003**, *299*, 1691–1693.

[41] We note that "triphos" has been used to described both "1,1,1-tris(diphenylphosphinomethyl)ethane" and "bis(diphenylphosphinoethyl)phenylphosphine" in the literature.

[42] (a) Huttner, G.; Strittmatter, J.; Sandhoefner, S. *Phosphorus Tripodal Ligands*. In *Comprehensive Coordination Chemistry II. Vol. 1., 2003,* pp. 297–322. DOI: 10.1016/B0-08-043748-6/01082-3. (b) Betley, T. A.; Peters, J. C. Dinitrogen Chemistry from Trigonally Coordinated Iron and Cobalt Platforms. *J. Am. Chem. Soc.* **2003**, *125*, 10782–10783.

[43] Güthner; T.; Mertschenk, B. *Cyanamides*. In *Ullmann's Encyclopedia of Industrial Chemistry*. Weinheim: Wiley-VCH, 2006. DOI: 10.1002/14356007.a08_139.pub2.

[44] Distonic radical cations is defined by IUPAC as a radical cation in which charge and radical sites are separated, see: Muller, P. *Pure &Appl. Chem.* **1994**, *66*, 1077–1184.

[45] Reactions using Bu_4NPF_6 in 4:1 MeCN/MeOH instead of Et_4NOAc in 4:1 NMP/MeOH also provide high yields of iminophosphorane **1** (specifically 76%), and thus DFT computations were performed using MeCN.

[46] Data based on using 4.59 V for the absolute potential of SHE in MeCN and a conversion from SHE to SCE by subtracting 244 mV from SHE potential. see: Marenich, A. V.; Ho, J.; Coote, M. L.; Cramer, C. J.; Truhlar, D. G. Computational electrochemistry: prediction of liquid-phase reduction potentials. *Phys. Chem. Chem. Phys.* **2014**, *16*, 15068–15106.

[47] Conversion of potential vs SCE to vs Fc/Fc^+ were accomplished by subtracting 0.38 V from the potentials vs SCE based on literature conversion factors, see: Pavlishchuk, V. V; Addison, A. W. Conversion constants for redox potentials measured versus different reference electrodes in acetonitrile solutions at 25°C. *Inorganica Chim. Acta* **2000**, *298*, 97–102.

[48] (a) A synthetic chemist's guide to electroanalytical tools for studying reaction mechanisms. Sandford, C.; Edwards, M. A.; Klunder, K. J.; Hickey, D. P.; Li, M.; Barman, K.; Sigman, M. S.; White, H. S.; Minteer, S. D. *Chem. Sci.* **2019**, *10*, 6404–6422. (b) Siu, J.; Sauer, G. S.; Saha, A.; Macey, R. L.; Fu, N.; Chauviré, T.; Lancaster, K. M.; Lin, S. *J. Am. Chem. Soc.* **2018**, *140*, 12511−12520.

[49] For an example of a domino electrolysis reaction, see previous reports on converting aldoximes to nitriles via oxidation to a nitrile oxide intermediate and subsequent reduction: (a) Shono, T.; Matsumura, Y.; Tsubata, K.; Kamada, T.; Kishi, K. Electroorganic chemistry. 116. Electrochemical transformation of aldoximes to nitriles using halogen ions as mediators: intermediary formation of nitrile oxides. *J. Org. Chem.* **1989**, *54*, 2249–2251. (b) Hartmer, M. F.; Waldvogel, S. R. Electroorganic Synthesis of Nitriles via a Halogen-Free Domino Oxidation-Reduction Sequence. *Chem. Commun.* **2015**, *51*, 16346−16348.

[50] For a 2nd example of a domino electrochemical reaction, see: Dong, X.; Roeckl, J. L.; Waldvogel, S. R.; Morandi, B. Merging shuttle reactions and paired electrolysis for reversible vicinal dihalogenations. *Science* **2021**, *371*, 507–514.

[51] Wu, T.; Moeller, K. D., Paired Electrolysis. In *Science of Synthesis: Electrochemistry in Organic Synthesis*, **2021**, *1*, 481. DOI: 10.1055/sos-SD-236-00331.

[52] Tolman, C. A. Steric effects of phosphorus ligands in organometallic chemistry and homogeneous catalysis. *Chem. Rev.* **1977**, *77*, 313–348.

[53] Gusev, D. G. Donor Properties of a Series of Two-Electron Ligands. *Organometallics* **2009**, *28*, 763–770.

[54] We note that limitations are known regarding the interpretation of TEP values, see: Cremer, D. Kraka, E. Generalization of the Tolman electronic parameter: the metal–ligand electronic parameter and the intrinsic strength of the metal–ligand bond. *Dalton Trans.* **2017**, *46*, 8323–8338.

[55] (a) Gilheany, D. G. No d Orbitals but Walsh Diagrams and Maybe Banana Bonds: Chemical Bonding in Phosphines, Phosphine Oxides, and Phosphonium Ylides. *Chem. Rev.* **1994**, *94*, 1339–1374. (b) Fey, N.; Orpen, A. G.; Harvey, J. N. Building ligand knowledge bases for organometallic chemistry: Computational description of phosphorus(III)-donor ligands and the metal–phosphorus bond. *Coord. Chem. Rev.* **2009**, *253*, 704–722.

[56] (a) Bandoli, G.; Bortolozzo, G.; Clemente, D. A.; Panattoni, C. Crystal and molecular structure of triphenylphosphine oxide. *J. Chem. Soc. A*, **1970**, 2778–2780. (b) Al-Farhan, K. A. Crystal structure of triphenylphosphine oxide. *J. Crystallogr. Spectrosc. Res.* **1992**, *22*, 687–689.

[57] Kashimura, S., Matsumoto, K. (2014). Electrogenerated Base. In: Kreysa, G., Ota, Ki., Savinell, R.F. (Eds) Encyclopedia of Applied Electrochemistry. Springer, New York, NY. https://doi.org/10.1007/978-1-4419-6996-5_354

[58] (a) Marsh, F. D.; Hermes, E. Cyanogen Azide. *J. Am. Chem. Soc.* **1964**, *86*, 4506–4507. (b) Goldsmith, Derek (2001). "Cyanogen azide". Encyclopedia of Reagents for Organic Synthesis. E-EROS Encyclopedia of Reagents for Organic Synthesis. DOI:10.1002/047084289X.rc268. ISBN 978-0471936237. (c) Marsh, F. D. Cyanogen azide. *J. Org. Chem.* **1972**, *37*, 2966–2969. (d) Robert Matyáš; Jiří Pachman (12 March 2013). Primary Explosives. Springer Science & Business Media. p. 111. (e) Michael L. Madigan (13 September 2017). First Responders Handbook: An Introduction, Second Edition. CRC Press. p. 170.

[59] Ihn, S.-G.; Lee, N.; Jeon, S. O.; Sim, M.; Kang, H.; Jung, Y.; Huh, D. H.; Son, Y. M.; Lee, S. Y.; Numata, M.; Miyazaki, H.; Gómez-Bombarelli, R.; Aguilera-Iparraguirre, J.; Hirzel, T.; Aspuru-Guzik, A.; Kim, S.; Le, S. An Alternative Host Material for Long-Lifespan Blue Organic Light-Emitting Diodes Using Thermally Activated Delayed Fluorescence. *Adv. Sci.* **2017**, *4*, 1600502.

TOC Graphic

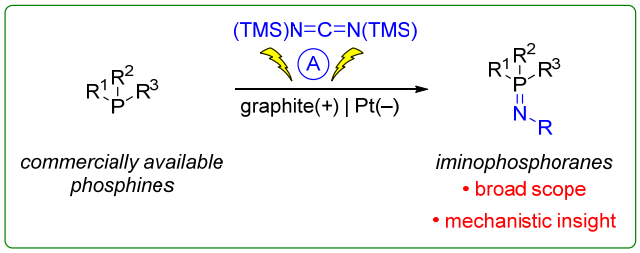
(TMS)N=C=N(TMS)
A
graphite(+) | Pt(–)
commercially available phosphines
iminophosphoranes
• broad scope
• mechanistic insight